Large parallel electric fields in the upward current region of the aurora: Evidence for ambipolar effects

A. J. Hull, J. W. Bonnell, and F. S. Mozer
Space Sciences Laboratory, University of California, Berkeley, California, USA

J. D. Scudder
Department of Physics and Astronomy, University of Iowa, Iowa City, Iowa, USA

C. C. Chaston
Space Sciences Laboratory, University of California, Berkeley, California, USA

Received 11 September 2002; revised 28 January 2003; accepted 3 April 2003; published 28 June 2003.

[1] Electric fields parallel to the magnetic field play a major role in the transport of mass, momentum, and energy in the auroral zone. In this paper we explore which terms of the steady state electron momentum equation are consistent with the large-amplitude, macroscopic parallel electric fields (~25 mV/m to 300 mV/m) measured by the electric field instrument on Polar in the upward current part of the auroral acceleration region. From a detailed analysis of eight events we found evidence suggesting that the large-amplitude, macroscopic parallel electric fields are ambipolar in character; namely, they are supported by electron pressure gradients present at the interface separating the relatively cold, dense ionospheric plasma from the hot, tenuous magnetospheric plasma in the auroral density cavity. These structures do not appear to be explained by purely propagating Alfvén waves. These large-amplitude, macroscopic parallel electric fields are likely to be a sheath field that forms at the boundary separating a high and low density plasma, similar to that encountered in laboratory experimental devices. *INDEX TERMS:* 2704 Magnetospheric Physics: Auroral phenomena (2407); 2712 Magnetospheric Physics: Electric fields (2411); 2736 Magnetospheric Physics: Magnetosphere/ionosphere interactions; 7815 Space Plasma Physics: Electrostatic structures; 7859 Space Plasma Physics: Transport processes; *KEYWORDS:* parallel electric fields, auroral acceleration, magnetosphere-ionosphere interactions, transport processes, electrostatic structures

Citation: Hull, A. J., J. W. Bonnell, F. S. Mozer, J. D. Scudder, and C. C. Chaston, Large parallel electric fields in the upward current region of the aurora: Evidence for ambipolar effects, *J. Geophys. Res.*, *108*(A6), 1265, doi:10.1029/2002JA009682, 2003.

1. Introduction

[2] Electric fields parallel to the magnetic field play a major role in the transport of mass, momentum, and energy in the auroral zone. Direct observations have revealed that the quasistationary parallel electric fields believed to be responsible for particle acceleration can be of large amplitude [e.g., *Mozer et al.*, 1980; *Mozer*, 1980; *Mozer and Kletzing*, 1998; *Mozer and Hull*, 2001; *Hull et al.*, 2000a; *Ergun et al.*, 2001; *Hull et al.*, 2003]. In particular, *Hull et al.* [2003] found 64 events in the upward current part of the auroral acceleration region, which contained macroscopic parallel electric fields ranging in amplitude from about 25 mV/m to 300 mV/m. The parallel electric field structures discussed in their study represented a significant fraction of the total electric field strength (with peak $E_\parallel/E_\perp$ ranging from ~0.25 to O(10)) and tended to occur at the edges of oppositely directed (converging) pairs of perpendicular electric field structures (often called electrostatic shocks) in a region where the gradients in the plasma density are quite large. *Hull et al.* [2003] found that the large parallel electric fields are more frequently observed at about 1.28 R_E altitude. These large-amplitude parallel electric fields lead to parallel potential drops that are localized in altitude (e.g., tens of kilometers as opposed to thousands of kilometers). The parallel electric field amplitudes were shown to be anticorrelated with the plasma density, with no apparent correlation with the current density [*Mozer and Hull*, 2001; *Hull et al.*, 2003]. *Hull et al.* [2003] suggested that the parallel electric fields can be explained by electron pressure gradient effects along the magnetic field separating plasma of different densities and temperatures. Highly localized, large-amplitude parallel electric fields have also been suggested in recent one-dimensional (1-D) kinetic models of the upward current part of the auroral acceleration region [*Ergun et al.*, 2000, 2002]. In particular, numerical solutions to 1-D Vlasov-Poisson equations using realistic boundary conditions recovered much of the properties of the observed field and particle distributions in the study by *Ergun et al.* [2002].

[3] From a fluid conservation law perspective, large-amplitude, macroscopic parallel electric fields can be sup-

0148-0227/03/2002JA009682$09.00

ported by a number of possible effects such as pressure gradients, anisotropy, inertia, and anomalous resistivity. Each of these effects can limit the plasma's ability to carry the current imposed somewhere in the magnetosphere, leading to certain characteristics of the parallel electric field that can be directly tested from observations. The purpose of this paper is to establish which of these effects is associated with large DC parallel electric fields via detailed analyses of events observed by Polar. This study is an extension of previous studies of large-amplitude macroscopic parallel electric fields observed by Polar [*Mozer and Kletzing*, 1998; *Mozer and Hull*, 2001; *Hull et al.*, 2003]. By emphasizing a conservation law perspective, our study provides a description of parallel electric fields that is complementary to that of recent studies [*Ergun et al.*, 2000, 2002], which emphasize a kinetic point of view. In section 3 we discuss the general theoretical framework under which comparisons are made using observations. The properties of a total of eight events with large DC parallel fields were analyzed and comparisons were made with the theoretical expectations developed in section 3. These events were selected from the previously compiled database of 64 events presented in the paper by *Hull et al.* [2003]. For the purposes of this study we chose events which had adequate particle sampling. The details of the plasma and field properties of three of the events characterized by different field geometries and plasma conditions are presented in section 4. The properties of a total of eight events with large DC parallel fields and comparisons with theoretical expectations are summarized in section 5. These eight events are representative of the majority of the events discussed in the previous study by *Hull et al.* [2003]. Our results suggest that the large DC parallel electric fields observed in the auroral acceleration region are balanced by pressure gradients (with the dominant contribution being from the density gradient component) present at the interface separating the relatively cold, dense ionospheric plasma and the hot, tenuous magnetospheric plasma. Mechanisms, such as electron inertia [e.g., *Rönnmark*, 1999] and the effects of mirroring magnetic fields on differential electron and ion anisotropy [e.g., *Alfvén and Fälthammer*, 1963] cannot explain these large-amplitude, macroscopic parallel electric fields, which lead to a large potential drop localized in a region that is roughly tens of kilometers in extent along the magnetic field. Moreover, tests suggest that these structures are not due to purely propagating Alfvén waves. A likely explanation is that the large parallel electric fields are a sheath field that forms at the boundary separating a high and low density plasma, similar to that encountered in laboratory experimental devices.

2. Instrumentation and Experimental Data Set

[4] In this study we analyze electric field data measured by the electric field instrument (EFI) on board Polar [*Harvey et al.*, 1995]. EFI is composed of three orthogonal sphere pairs that measure the electric field vector. The double probes in the spin plane have a separation of 100 m and 130 m, respectively. The third pair of spheres lie along the spin axis and are held 14 m apart by rigid booms. The electric field is sampled at a rate of 40 vectors per second. Spacecraft floating potential data (used as a proxy for the plasma density) is sampled at 2.5 Hz in normal telemetry mode. High-time-resolution magnetic field data at 8 vectors per second were provided by the Polar magnetic field experiment (MFE) [*Russell et al.*, 1995].

[5] High-time-resolution (1.15 s) electron and ion data used in this paper were measured by the DuoDeca Electron Ion Spectrometer (DDEIS) component of the HYDRA instrument on board Polar [*Scudder et al.*, 1995]. The DDEIS measures counts in 12 look directions with narrow field of view ($8^\circ \times 8^\circ$) and energy bandwidth of $\Delta E/E = 6\%$, alternating between electron and ion samples in subsequent energy sweeps (1.15 s) from 12 eV to 18 keV. The electron data have been corrected for spacecraft floating potential using direct measurements from EFI, prior to computing the electron moment quantities.

3. Electron Fluid Considerations

[6] Parallel electric fields can be balanced by a number of possible effects, including pressure gradients, inertia, and resistivity, the process of which is succinctly summarized by the generalized Ohm's law. Certainly, Ohm's law does not shed light on the detailed particle dynamics, essential to understanding the formation of the parallel electric field, including accessibility of particle orbits to the phase space boundaries that define the system. This shortcoming does not make Ohm's law inferior to such a detailed particle description. Namely, the generalized Ohm's law is a conservation law restatement of the collective response of the plasma to the parallel electric field that must necessarily be maintained by any detailed particle description, and more importantly, such a conservation law description is amenable to comparison with direct observations.

[7] Alternative conservation relations for the parallel electric field that are equivalent to the generalized Ohm's law can be obtained from the electron or ion momentum equations. In this paper we use the electron momentum equation to explore which effect (e.g., pressure gradient, anisotropy, inertia) balances the large amplitude, macroscopic parallel electric fields observed in the upward current portion of the auroral acceleration region [e.g., *Mozer and Kletzing*, 1998; *Mozer and Hull*, 2001; *Hull et al.*, 2003]. We use the electron momentum equation in our study because of its relative interpretive simplicity (e.g., use of the electron momentum equation avoids the added complexity of finite Larmor radius effects inherent to the ion momentum equation). There is also the added advantage that the full 3-D electron distributions are well measured over the regions of interest, yielding accurate moments that can be used in comparisons with theory. The ions on the other hand are not well measured outside the auroral density cavity because a significant fraction gets reflected by the spacecraft floating potential, making comparisons based on the ion momentum equation difficult if not impossible.

[8] The electron momentum equation yields the following expression for the parallel electric field:

$$E_{\parallel} = -\frac{m_e}{e}\left(\frac{\partial U_{\parallel}}{\partial t} + \mathbf{U_e}\cdot\nabla\mathbf{U_e}\right)\cdot\hat{\mathbf{b}} - \frac{1}{eN_e} \cdot\left[\frac{\partial P_{e\parallel}}{\partial S_{\parallel}} - \left(P_{e\parallel} - P_{e\perp}\right)\frac{\partial \ln B}{\partial S_{\parallel}}\right] + R_{\parallel}, \quad (1)$$

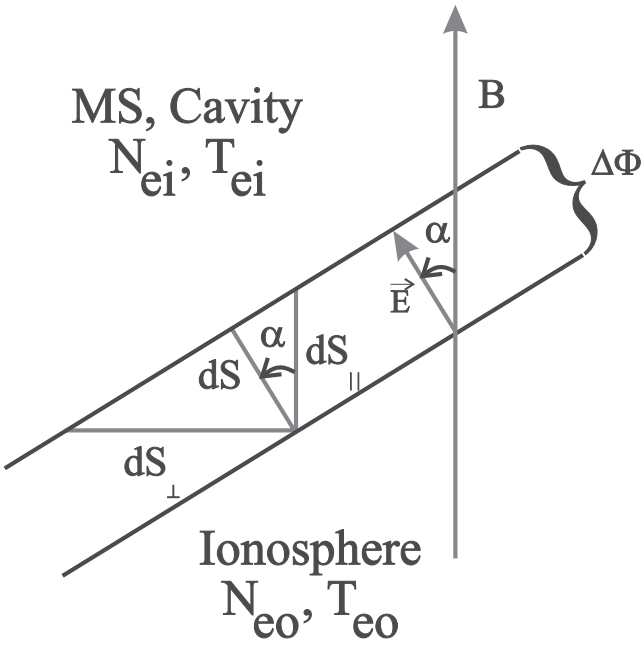

Figure 1. Model of the transition between the relatively cold, dense ionospheric plasma and the hot, tenuous magnetospheric plasma. The transition is modeled as a time stationary, planar layer. The layer is assumed to be defined by the electric field (e.g., gradient in potential), which in the presence of a significant parallel component will be inclined at an angle α with respect to the background magnetic field.

where m_e is the electron mass, e is the electron charge, N_e is the electron density, $\mathbf{U_e}$ is the electron bulk velocity, $\hat{\mathbf{b}}$ is the magnetic field unit vector, B is the magnitude of the magnetic field, $P_{e\|}$ and $P_{e\perp}$ are the parallel and perpendicular electron pressure, and $R_\|$ is often modeled in a collisionless plasma as $\eta_a J_\|$, where η_a is the anomalous resistivity and $J_\|$ is the parallel current density. In equation (1) the partial derivative of a quantity X along the magnetic field is defined as $\hat{\mathbf{b}} \cdot \nabla X \equiv \partial X/\partial S_\|$. Equation (1) is obtained by taking the first moment of the Vlasov equation for the electrons under the assumption that the electron pressure is gyrotropic and projecting the resulting electron momentum transport equation along $\hat{\mathbf{b}}$. The first two terms represent electron inertial effects, the third term reflects parallel fields supported by parallel electron pressure gradients along the magnetic field, the fourth represents electron pressure anisotropy, and the last term represents effects associated with fluctuating fields.

[9] To bring theory into contact with observed quantities, we model the layer containing the macroscopic parallel electric field as a time stationary, planar sheath. The time stationary assumption is motivated from the study by *Hull et al.* [2003], who provided evidence suggesting that the macroscopic parallel electric field signatures are static structures convecting by the spacecraft at the spacecraft velocity. Thus we take $(m_e/e)\partial U_\|/\partial t = 0$ in equation (1). The layer geometry motivated by observations [*Mozer and Kletzing*, 1998; *Hull et al.*, 2003] is given in Figure 1. The events discussed in this paper are observed in the southern auroral acceleration region. Thus the magnetic field points upward, away from Earth as depicted in Figure 1. The layer contains an electric field inclined at an angle α with respect to the magnetic field, which gives rise to a net potential drop $\Delta\Phi$. In traversing the layer from the ionospheric side to inside the cavity, the plasma density decreases ($N_{eo} > N_{ei}$) and the electron temperature increases ($T_{eo} < T_{ei}$).

3.1. Relative Importance of Various Effects

[10] Observations [e.g., *Mozer and Kletzing*, 1998; *Hull et al.*, 2003] suggest regions containing the parallel electric fields are associated with strong density gradients, with only a moderate gradient in the electron temperature. In addition to being localized in latitude, observations also suggest that the parallel electric fields and hence the associated parallel potential drops are localized in altitude. No noticeable magnetic field variations are observed to occur within the layer containing the parallel electric field. These observational constraints allow us to simplify equation (1).

[11] The inertial term in equation (1) simplifies to $-(m_e/e)(\mathbf{U_e} \cdot \nabla \mathbf{U_e}) \cdot \hat{\mathbf{b}} = -(m_e/e)U_{e\|}\partial U_{e\|}/\partial S_\|$ in the geometry depicted in Figure 1. Using the field line conservation constraint $\Gamma = N_e U_{e\|}/B = const$ (which is equivalent to $J_\|/B = const$ along a flux tube if the electrons carry all the current) and the fact that the logarithmic derivative of the magnetic field is negligible in comparison with the logarithmic derivative of the density (e.g., the scale length over which the density varies is typically $L_N \equiv |S_\|/\partial \ln N_e| \sim 10$ km, whereas the scale length of the variation of the magnetic field is $L_B \equiv |\partial S_\|/\partial \ln B| \sim 1000$ km), the inertial term can be expressed as follows:

$$-\frac{m_e}{e}U_{e\|}\frac{\partial U_{e\|}}{\partial S_\|} = \frac{m_e}{e}U_{e\|}^2\left[\frac{\partial \ln N_e}{\partial S_\|} - \frac{\partial \ln B}{\partial S_\|}\right] \approx \frac{m_e}{e}U_{e\|}^2\frac{\partial \ln N_e}{\partial S_\|}. \quad (2)$$

The parallel pressure gradient term in equation (1) is approximately given by $(1/eN_e)(\partial P_{e\|}/\partial S_\|) \approx (T_{e\|}/e)(\partial \ln N_e/\partial S_\|)$. Thus under the assumption that the layers containing the parallel electric field are time stationary, thin, planar layers and that the gradient in the electron density is much larger than the electron temperature gradient, equation (1) can be approximated as follows:

$$E_\| = \frac{m_e}{e}U_{e\|}^2\frac{\partial \ln N_e}{\partial S_\|} - \frac{T_{e\|}}{e}\frac{\partial \ln N_e}{\partial S_\|} + \frac{1}{e}\left(T_{e\|} - T_{e\perp}\right)\frac{\partial \ln B}{\partial S_\|} + \eta J_\|. \quad (3)$$

[12] In equation (3) the contribution of the electron pressure anisotropy term relative to the pressure term scales as

$$\left|\frac{\left(P_{e\|} - P_{e\perp}\right)\left(\partial \ln B/\partial S_\|\right)}{\left(\partial P_{e\|}/\partial S_\|\right)}\right| \sim \left|\left(1 - \frac{T_{e\perp}}{T_{e\|}}\right)\frac{\left(\partial \ln B/\partial S_\|\right)}{\left(\partial \ln N_e/\partial S_\|\right)}\right|$$

$$\sim \left|\frac{\left(\partial \ln B/\partial S_\|\right)}{\left(\partial \ln N_e/\partial S_\|\right)}\right| = \frac{L_N}{L_B} \ll 1. \quad (4)$$

Thus we can neglect contributions due to electron pressure anisotropy.

[13] The electron inertial term in equation (3), if it were the dominant effect, would lead to a parallel electric field which points downward, toward Earth, which is contrary to observations in regions of upward current. Nevertheless, the electron inertial term could provide nonnegligible corrections if it were competitive with other effects that could be supporting $E_{\parallel}$, such as the parallel pressure gradient. The contribution of the inertial term relative to the pressure term scales as:

$$\frac{(m_e/e)U_{e\parallel}\left(\partial U_{e\parallel}/\partial S_{\parallel}\right)}{(1/eN_e)\left(\partial P_e/\partial S_{\parallel}\right)} \sim \frac{m_e U_{e\parallel}^2\left(\partial \ln N_e/\partial S_{\parallel}\right)}{T_{e\parallel}\left(\partial \ln N_e/\partial S_{\parallel}\right)} \sim \frac{m_e U_{e\parallel}^2}{T_e} \equiv M_{the}^2, \tag{5}$$

where $M_{the} = U_{\parallel}/V_{the}$ is the electron thermal Mach number. The electron inertial effects can be neglected provided the parallel flow is sufficiently subthermal. An upper bound estimate of the parallel electron bulk speed can be obtained from estimates of the parallel current density by assuming that the electrons carry all of the current. The distribution of $J_{\parallel}$ estimated from magnetic field data and corresponding distribution upper bound estimates of the parallel electron bulk speeds for the 64 parallel electric field events compiled by *Hull et al.* [2003] are displayed in Figures 2a and 2b, respectively. The current density and parallel bulk speed are found to have respective median values of 0.12 μA m^{-2} and 650 km s^{-1}. The electron temperatures in the vicinity of the parallel electric field measurements are typically observed to be of the order of $\sim$1 keV, which yield a typical thermal speed of 1.3×10^3 km s^{-1}. The resulting distribution of M_{the} is given in Figure 2c. It is clear from Figure 2c that $M_{the}^2 \ll 1$, and thus the electron inertial term is negligible in comparison with the electron parallel pressure gradient.

[14] The saturated state of various wave instabilities could lead to fluctuating fields of sufficient amplitude to affect momentum transport along a flux tube. In analogy to collision dominated plasmas, the cumulative effects of the AC fields are often simplified, without justification, as a resistive drag term in the electron momentum transport equation, with the anomalous resistivity defined as:

$$\eta_a = \frac{\nu_a}{\epsilon_0 \omega_{pe}^2}, \tag{6}$$

where ω_{pe} is the electron plasma frequency and ν_a is the effective collision frequency of the wave mode responsible for the source or sink of electron momentum. In this paper we adopt this formalism in describing the effects due to wave-particle interactions, keeping in mind that a different relationship between $R_{\parallel}$ and other fluid variables may be more appropriate.

[15] In the auroral acceleration region ion cyclotron [e.g., *Mozer et al.*, 1977; *Hudson et al.*, 1978; *Kintner et al.*, 1979; *Ergun et al.*, 1998; *Cattell et al.*, 1998a] and ion acoustic waves [e.g., *Cattell et al.*, 1998b] are suggested as possible modes that can contribute to anomalous resistivity. At the altitudes over which large parallel electric fields were observed by Polar, ion acoustic waves are expected to be strongly damped since $T_e \sim T_i$ and the current is not sufficient for the waves to grow to significant amplitudes to affect the plasma as they traverse the thin layers containing significant parallel electric fields. Ion cyclotron waves with a significant parallel electric field component have been observed to occur over intervals which only partially overlap regions containing large DC parallel electric fields [*Hull et al.*, 2003], suggesting that ion cyclotron waves are not the source of the large-amplitude, macroscopic parallel electric field signatures. The effective collision frequency of ion cyclotron waves is typically of the order of a fraction of

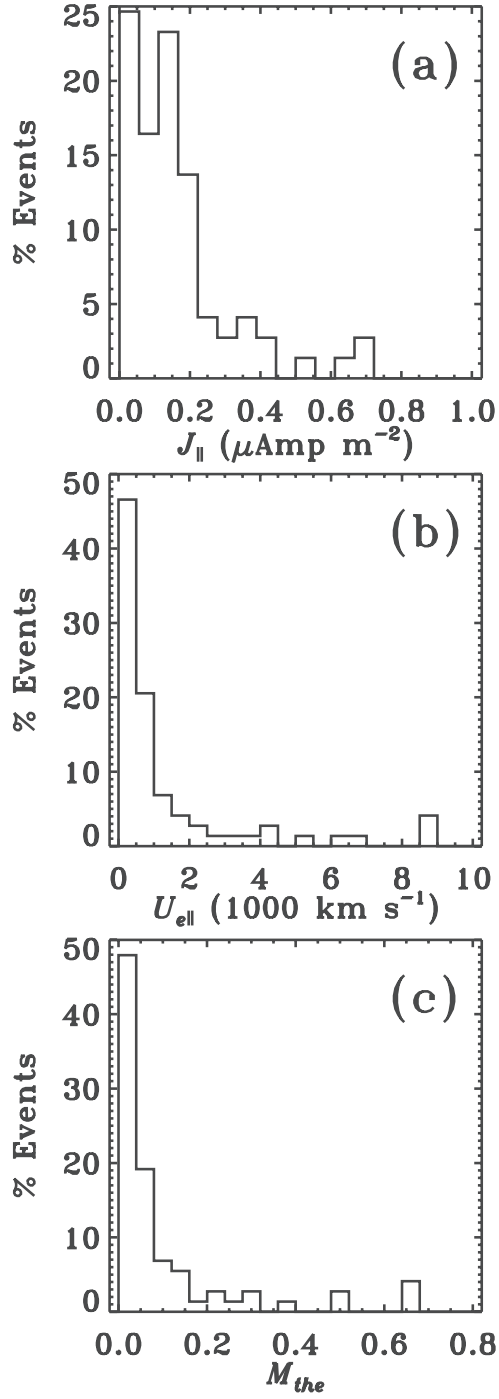

Figure 2. Shows (a) the distribution of $J_{\parallel}$ estimated from magnetic field measurements, (b) resulting parallel electron bulk speed assuming the electrons carry all the current, and (c) $M_{the} = U_{\parallel}/V_{the}$ for the database of events compiled by *Hull et al.* [2003].

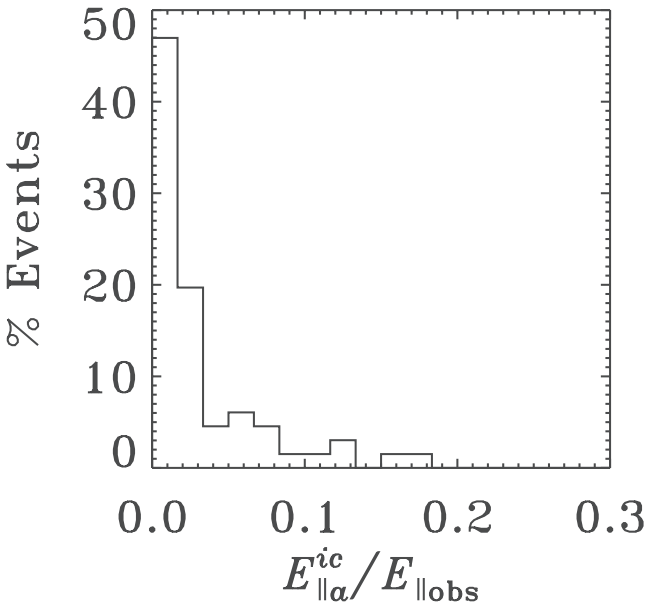

Figure 3. Shows a histogram of the ratio between the effective parallel electric field that may be induced by ion cyclotron waves and the peak amplitude of observed macroscopic parallel electric fields.

the ion cyclotron frequency [e.g., *Treumann and Baumjohann*, 1997]. A gross overestimate of the parallel electric field $E^{ic}_{\|a}$ that can be supported by ion cyclotron waves whenever present can be obtained by assuming the effective anomalous collision frequency is given by $\nu^{ic}_a \sim \Omega_{ci}$. Figure 3 shows a histogram of the ratio between $E^{ic}_{\|a}$ and the peak amplitude of macroscopic parallel electric fields $E_{\|obs}$ observed in the events featured in the study by *Hull et al.* [2003]. The fact that $E^{ic}_{\|a}$ is only a small fraction of $E_{\|obs}$ suggests that ion cyclotron waves if present cannot support such large-amplitude, macroscopic parallel electric fields. Thus we will neglect effects of wave-particle interactions.

[16] Neglecting pressure anisotropy, inertial, and resistive effects, the parallel electric field is ambipolar in character and is represented by the following expression:

$$E_{\|} = -\frac{1}{eN_e}\nabla P \cdot \hat{\mathbf{b}} = -\frac{1}{eN_e}\frac{\partial P_e}{\partial S_{\|}}, \tag{7}$$

where $P_e = N_e T_e$ is the isotropic electron pressure. The concept that parallel electric fields can be ambipolar in character is not novel. Early studies [*Pannekoek*, 1922; *Rosseland*, 1924] have realized the importance of ambipolar electric fields (including the parallel component) in maintaining quasineutrality in an inhomogeneous plasma in the context of solar wind acceleration. In addition, evidence that ambipolar effects support parallel electric fields has recently been established at the magnetopause [*Scudder et al.*, 2002] and has been inferred at collisionless shocks [e.g., *Goodrich and Scudder*, 1984; *Scudder et al.*, 1986; *Hull et al.*, 2000b]. Below, we provide eight examples of large-amplitude, macroscopic parallel electric fields observed in the auroral acceleration region by Polar that appear to be supported by ambipolar effects.

3.2. An Approximate Expression for the $E_{\|}$

[17] Polar's orbital velocity has significant components both along and transverse to the magnetic field, allowing for an assessment of both the parallel and perpendicular gradients. However, the sampling by the HYDRA instrument on Polar is too coarse to establish the detailed variation of the electron distribution and hence electron moments within the layer proper, thus we seek an approximate expression for the parallel electric field which depends on asymptotic values. An approximate expression can be obtained by differencing equation (7) across the layer under the assumption that the density gradient term is the most important term which yields:

$$E_{\|} \approx -\frac{T_e}{e}\frac{\partial \ln N_e}{\partial S_{\|}} \approx \frac{\langle T_e \rangle}{e\delta S_{\|}} \ln\left(\frac{N_{eo}}{N_{ei}}\right), \tag{8}$$

where $\langle T_e \rangle = (T_{eo} + T_{ei})/2$ is the average electron temperature, $\delta S_{\|}$ is the thickness of the layer along the magnetic field, N_{eo} is the electron density outside the cavity on the ionospheric side, and N_{ei} is the electron density in the cavity on the magnetospheric side. Given the asymptotic values for the electron density, the average electron temperature, and an estimate of the parallel thickness of the layer, equation (8) at best gives an estimate of the average parallel electric field within the layer, which can be tested with observations.

3.3. Determination of Layer Geometry and Thickness

[18] To determine the parallel and perpendicular scale of the sheath, we need to determine the sheath normal. The normal is determined by finding the eigenvectors and associated eigenvalues of the covariance matrix of the 3-D electric field given by:

$$M_{\alpha\beta} = \langle E_\alpha E_\beta \rangle - \langle E_\alpha \rangle \langle E_\beta \rangle. \tag{9}$$

The eigenvector associated with maximum variance is the normal. Boxcar averaging was applied to some of the examples to remove higher-frequency content, which can affect the boundary normal determinations. Significant variation in advection velocity and/or magnetic field across the structure can also seriously impact the value of $M_{\alpha\beta}$, giving inaccurate results. However, such an effect is negligible across the highly localized parallel electric field structures we analyze below, across which the magnetic field vector is approximately constant.

[19] Given the normal and assuming the structures are time stationary, the layer thicknesses were estimated from

$$dS = \mathbf{v_{S/C}} \cdot \hat{\mathbf{n}}\, dt, \tag{10}$$

where $\mathbf{v_{S/C}}$ is the spacecraft velocity vector, $\hat{\mathbf{n}}$ is the normal, and dt is the duration of the transition layer. The parallel and perpendicular thicknesses are given by $dS_{\|} = dS/\cos\alpha$ and $dS_{\perp} = dS/\sin\alpha$, where α is the angle between the inward pointing normal and the magnetic field (see Figure 1).

4. Comparisons With Observations

[20] The process of identifying and validating parallel electric fields observed by Polar has been discussed elsewhere [e.g., *Mozer and Kletzing*, 1998; *Scudder et al.*, 2002; *Hull et al.*, 2003]. Thus in this section we show the results

of our analysis of three events containing large-amplitude, macroscopic parallel electric field structures encountered by Polar in the southern auroral acceleration region. In this section we discuss in detail the properties of three of the events containing large-amplitude, macroscopic parallel electric field structures encountered by Polar in the southern auroral acceleration region. The events presented in this section are taken from different field geometry and plasma conditions. The results of our analysis suggest that electron pressure gradients at the interface between high and low density plasma support the large-amplitude macroscopic parallel electric fields that occur in the auroral acceleration region.

4.1. 25 September 1996 Event

[21] An example of a southern auroral zone crossing on 25 September 1996 is illustrated in Figure 4. Polar was near midnight at a geocentric distance of roughly 1.87 R_E. The event occurred during relatively quiet magnetospheric conditions, with the 3 hour K_p index being 2-. Figure 4a depicts the electron density indicated by red dashes determined from electron counts measured by the HYDRA DDEIS detectors. The width of the red dashes corresponds to the 1.15 s accumulation time of electron counts used in a given density determination. Also shown in Figure 4a is the density estimated from spacecraft potential measurements (black curve) using a density-potential relation established over the current epoch. Throughout most of the interval, the spacecraft potential measurements provide higher time resolution estimates of the density that are in good quantitative agreement with that determined from electron data, when averaged over the 1.15 s HYDRA DDEIS accumulation time. The large discrepancy at ~2346:40 UT is attributed to undersampling of electron phase space, associated with gaps in the HYDRA detector sampling. These kinds of discrepancies are easily identified via close inspection of the electron distribution function measurements (figure not shown).

[22] In Figure 4a, a region of depressed density is apparent in the interval from ~2346:42 UT to ~2347:47 UT, reaching an average density of ~0.12 cm^{-3}. Outside the cavity, the density is found to be ~0.6 cm^{-3} to ~0.8 cm^{-3}. The electron temperature given in Figure 4b is slightly enhanced within the density cavity relative to the temperature outside the cavity.

[23] The electric fields are displayed in Figures 4c–4e. The electric fields are given in a magnetic field aligned coordinate system in which the z-axis represents the direction along the magnetic field, the x-axis is in the local plane of curvature of the magnetic field and points equatorward, and the y-axis completes the orthonormal set and points in the magnetic westward direction. A parallel electric field signature (Figure 4e) with peak amplitude of 150 mV/m is observed near 2347:45 UT. The parallel electric field signature is coincident with a large perpendicular electric field signature (see Figures 4c–4d) with peak amplitude ~400 mV/m and occurs in a region characterized by a sharp density gradient. The increasing slope in the east-west perturbation magnetic field ΔB_Y (Figure 4f) suggests that parallel electric field signature is in a region of upward field aligned current. No noticeable magnetic field intensity variations are observed to occur in association with the parallel electric field within the layer, which suggests that the signatures are electrostatic. Figure 4g, which depicts the plasma potential Φ_{PL} (defined as $\Phi_{PL} = -\int \mathbf{E} \cdot \mathbf{dl}$), suggests a ~1–3 kV parallel potential drop below Polar in the regions of depressed density.

[24] Spectrograms of ion differential energy flux for pitch angle ranges from 0°–30° (upward) and 150°–180° (downward) are given in Figures 4h and 4i, respectively. Similarly, electron spectrograms for pitch angle ranges from 0°–30° (upward) and 150°–180° (downward) are shown in Figures 4j and 4k, respectively. The electron and ion spectrograms have been corrected for spacecraft floating potential using direct measurements from EFI. The gray background in Figures 4h–4k indicates gaps in the detector sampling. The gaps that occur every 1.15 s are the result of HYDRA's DDEIS mode of operation, which alternates between electron and ion samples in subsequent energy sweeps. The occasional gaps that occur in energy represent an absence of a measurement in a given 30° pitch-angle swath over a given energy sweep interval shown in Figures 4h–4k. Field-aligned ion beams with mean energy of ~1–3 keV appear in regions of depressed density, with little or no ions seen in the high density regions in Figures 4h and 4i. The variations in the ion beam energy appears to be consistent with the variations in Φ_{PL} depicted in Figure 4g, which is in accordance with an electrostatic description. Precipitating electrons are observed simultaneously with the upgoing ion beams (Figure 4k). In the high density regions, electrons up to keV energies are apparent. Dropouts in the upgoing electron differential energy flux at energies below ~1–3 keV within the density cavity (between ~2346:43 and ~2347:47 UT) in Figure 4j signify the existence of a parallel potential at altitudes below the spacecraft, which prevents electrons of ionospheric origin with energies below ~1–3 keV from accessing this altitude. Enhancements in the electron beam energies just outside the cavity (e.g., 23:47:45–2348:00 UT) relative to those within the cavity are consistent with parallel acceleration by a ~1–3 keV potential.

[25] We applied a variance analysis to the electric fields that occur at the right boundary of the density cavity (near 2347:47 UT) to determine the boundary normal. The variance analysis yielded a boundary normal $\hat{\mathbf{n}} = (-0.906, 0.338, 0.253)$ in the field-aligned coordinate system defined above. The normal is inclined at an angle $\alpha = 75.4°$, with respect to the magnetic field vector. Given the normal to the boundary and assuming the structure is convecting by the spacecraft at the spacecraft speed, the thickness of the layer is estimated to be 5.7 km, yielding values for the thicknesses parallel and perpendicular to the magnetic field of 23 km and 6.0 km, respectively. The temperature inside the cavity is about 1 keV and the temperature outside the cavity to the right of the parallel electric field signature is found to be 700 eV, yielding an average temperature $\langle T_e \rangle = 850$ eV. In addition the ratio of the density outside the cavity to that within the cavity is $N_o/N_i = 5$. Using these values in equation (8) yields an estimate of the parallel electric field $\langle E_{\|} \rangle^{\text{pred}} \approx 59 \pm 10$ mV/m. This compares favorably with the parallel electric field averaged over the layer which was found to be $\langle E_{\|} \rangle^{\text{obs}} = 50$ mV/m.

4.2. 2 April 1996 Event

[26] In the same format of the previous example, Figure 5 gives field and particle data for a southern crossing near

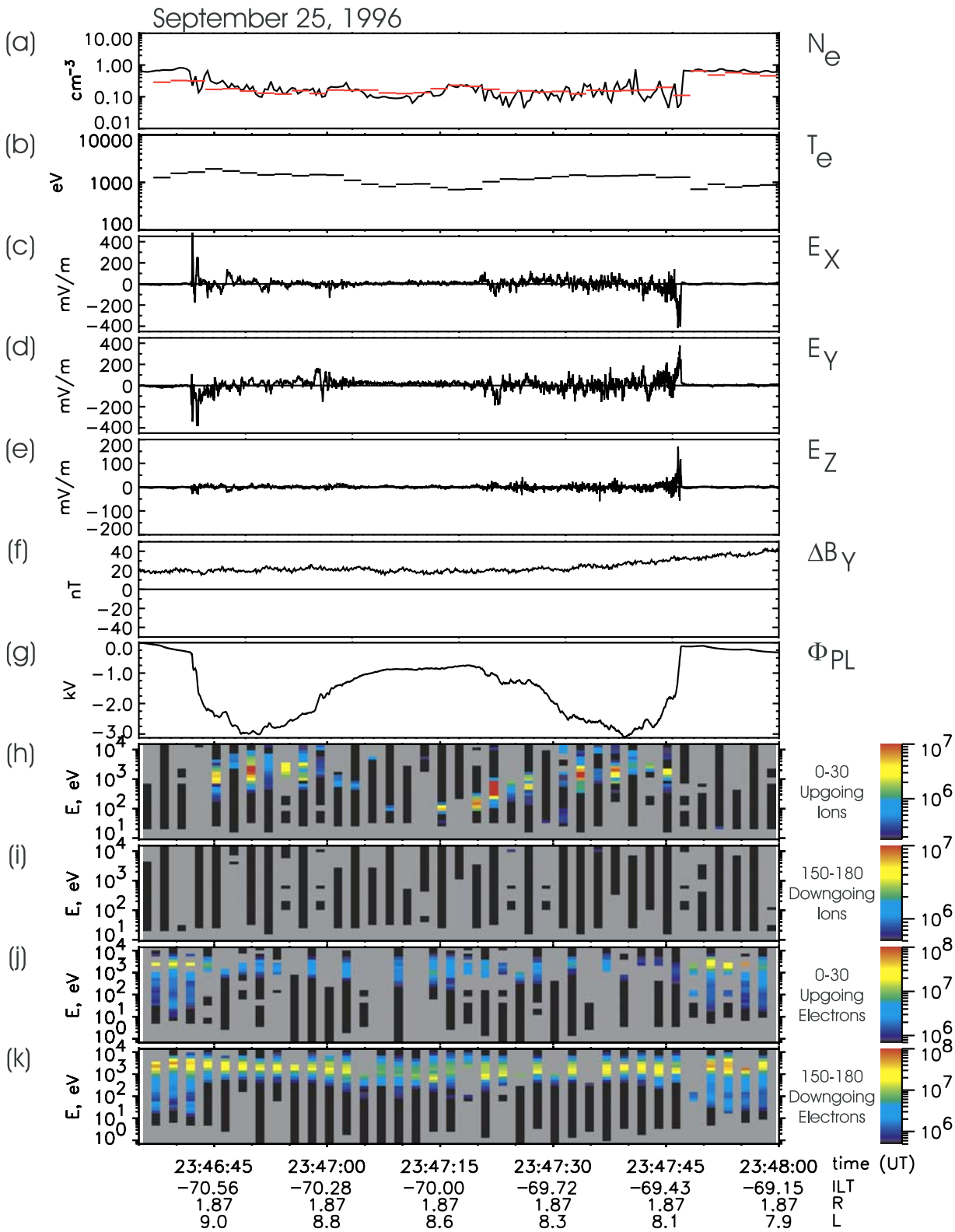

Figure 4. Depicts a southern auroral zone crossing near midnight on 25 September 1996. Shown are (a) electron density, (b) electron temperature, (c)–(e) the components of the electric field vector in field-aligned coordinates, (f) the east-west perturbation magnetic field, (g) the plasma potential, (h)–(i) spectrograms of field-aligned and field-opposed differential ion energy flux, respectively, and (j)–(k) spectrograms of field-aligned and field-opposed differential electron energy flux.

local midnight on 4 April 1996. The time interval is characterized by K_p index of equation (2). Figure 5a shows profiles of the density derived from electron data (red dashes) and density estimated from spacecraft potential (black curve) using a density-potential relation derived from data sampled over the entire day. The two density profiles agree quite well in the high density regions, whereas in the cavity regions they depart by as much as a factor of 2 in magnitude. The discrepancy between the two estimates of density in the cavity is due to the statistical density-potential relation's dependence on temperature [*Escoubet et al.*, 1997]. Nevertheless, the spacecraft potential measurements provide good qualitative high-time-resolution estimates of the density. In particular, the density estimated from spacecraft potential measurements reveal the presence of two regions of depressed density, one which occurs in the interval from ~2044:28 UT to ~2044:46 UT and the other occurring in the interval from ~2044:47 UT to ~2044:57 UT. These two separate depressed regions are difficult to identify in the electron moment density trace because the electron measurements are aliased over the short-duration, high-density region at ~2044:46 UT to ~2044:47 UT. According to the electron measurements, the density in the cavity is 0.07 cm^{-3} (0.04 cm^{-3} estimated from spacecraft potential measurements) and outside the cavity the density reaches a value of 0.2 cm^{-3}. The electron temperature is enhanced in the density cavity region, peaking at a value of 130 eV.

[27] A 250 mV/m amplitude parallel electric field exists (Figure 5e), with little or no $E_\perp$ (see Figures 5c and 5d). The peak $E_\parallel/E_\perp$ ratio corresponding to the large parallel field signature is roughly 8. The parallel electric field signature occurs in a region containing a sharp density gradient, which, as stated above, is more apparent in the density estimated from spacecraft potential measurements Figure 5a. The entire region is characterized by an upward field aligned current estimated to be ~0.01 $\mu A\ m^{-2}$ from ΔB_Y given in Figure 5f. The sampling by HYDRA is too coarse to establish the particle properties within the parallel electric field signature, though there are upgoing ions and downgoing electrons in the vicinity of the $E_\parallel$ event (see Figures 5h–5k). The upgoing ion beams are quite narrow in pitch angle in this event and HYDRA, with gaps in its angular sampling, captures the narrow beam only occasionally through the interval, when one of the pairs of detectors is nearly aligned (within 30°) along the magnetic field line. Dropouts in the upgoing electron differential energy flux seen between 2044:28 and 2044:46 UT at energies up to ~100–200 eV in Figure 5j signify the existence of a parallel potential below the spacecraft, which prevents electrons of ionospheric origin from accessing this altitude. It is difficult to assess whether the upgoing electron differential energy flux between ~2044:47 UT to ~2044:57 UT is consistent with a parallel potential below the Polar because of gaps in the HYDRA detector energy sampling.

[28] Variance analysis applied to the electric field data over the interval containing the parallel field signature yielded a boundary normal $\hat{\mathbf{n}}$ = (−0.110,−0.145, 0.983) which is nearly aligned along the magnetic field vector. The angle between the normal and the magnetic field is α = 11.0°. The parallel and perpendicular thicknesses are estimated at 0.82 km and 4.4 km, respectively. The average electron temperature was relatively cold ($\langle T_e \rangle$ = 90 eV) and the density ratio was estimated at 2.9 from the electron moment data. The predicted value of the parallel electric field was found to be $\langle E_\parallel \rangle^{\text{pred}} \approx 117 \pm 77$ mV/m (176 mV/m using spacecraft potential density estimates), which is consistent with $\langle E_\parallel \rangle^{\text{obs}}$ = 80 mV/m.

4.3. 30 June 1996 Event

[29] Plasma and field data corresponding to a parallel electric field event encountered by Polar in the southern auroral zone near dusk on 30 June 1996 is given in Figure 6 in the same format as used for the previous events. The three hour averaged K_p index was 1+, indicating that the event occurred during quiet magnetospheric conditions. This event is of particular interest because the parallel and perpendicular electric field signatures are of similar amplitudes. The electron density shown in Figure 6a makes a transition from 1.3 cm^{-3} in the high-density region at ~0416:15 UT to 0.16 to 0.3 cm^{-3} in the auroral cavity region (0416:25 UT to 0417:08 UT) and then returns to 1.3 near 0417:08 UT. A second region of low density occurs at times ≳0417:10 UT.

[30] The parallel electric field signature, which has a peak amplitude of 350 mV/m, occurs at ~0417:07 UT in the region characterized by a sharp gradient in the plasma density (see Figure 6e). The parallel electric field signature is nearly coincident with large-amplitude perpendicular fields characterized by peak amplitudes of 400 mV/m (See Figures 6c–6d). The decreasing value of ΔB_Y (Figure 6f) with increasing invariant latitude suggests that the event is characterized by an upward field-aligned current ($J_\parallel$ = 0.17 $\mu A\ m^{-2}$). The regions of depressed density are characterized by upward field aligned ion beams with peak energies reaching 5 to 6 keV (Figures 6h and 6i) and precipitating electrons (Figures 6j and 6k). The variations in the plasma potential (Figure 6g) are in rough accord with the beam energies of the ions. Dropouts in the upgoing electron differential energy fluxes within the density cavity regions between 0416:25 UT to 0417:08 UT at energies below a few keV indicate the existence of a field-aligned potential drop below the spacecraft.

[31] The variance analysis applied to electric field data, sampled over the interval where $E_\parallel$ occurred, yielded a boundary normal $\hat{\mathbf{n}}$ = (0.688, 0.459, 0.562), which is inclined at an angle α = 55.8° with respect to the magnetic field vector. The parallel and perpendicular thicknesses are 8.2 km and 5.6 km, respectively. The average temperature was estimated at 250 eV and the density ratio is roughly 8.6. Using these values in equation (8) yields a parallel electric field $\langle E_\parallel \rangle^{\text{pred}} \approx 66 \pm 40$ mV/m, which is in good agreement with the observed average value of parallel field in the layer which is found to be $\langle E_\parallel \rangle^{\text{obs}}$ = 102 mV/m. The favorable agreement between the predicted value and the observed average value suggests that the parallel electric field is supported by the pressure gradient separating the high and low density plasma.

5. Discussion

[32] In this study we characterized and analyzed a total of eight events containing significant parallel electric fields encountered by Polar in the southern auroral zone. These

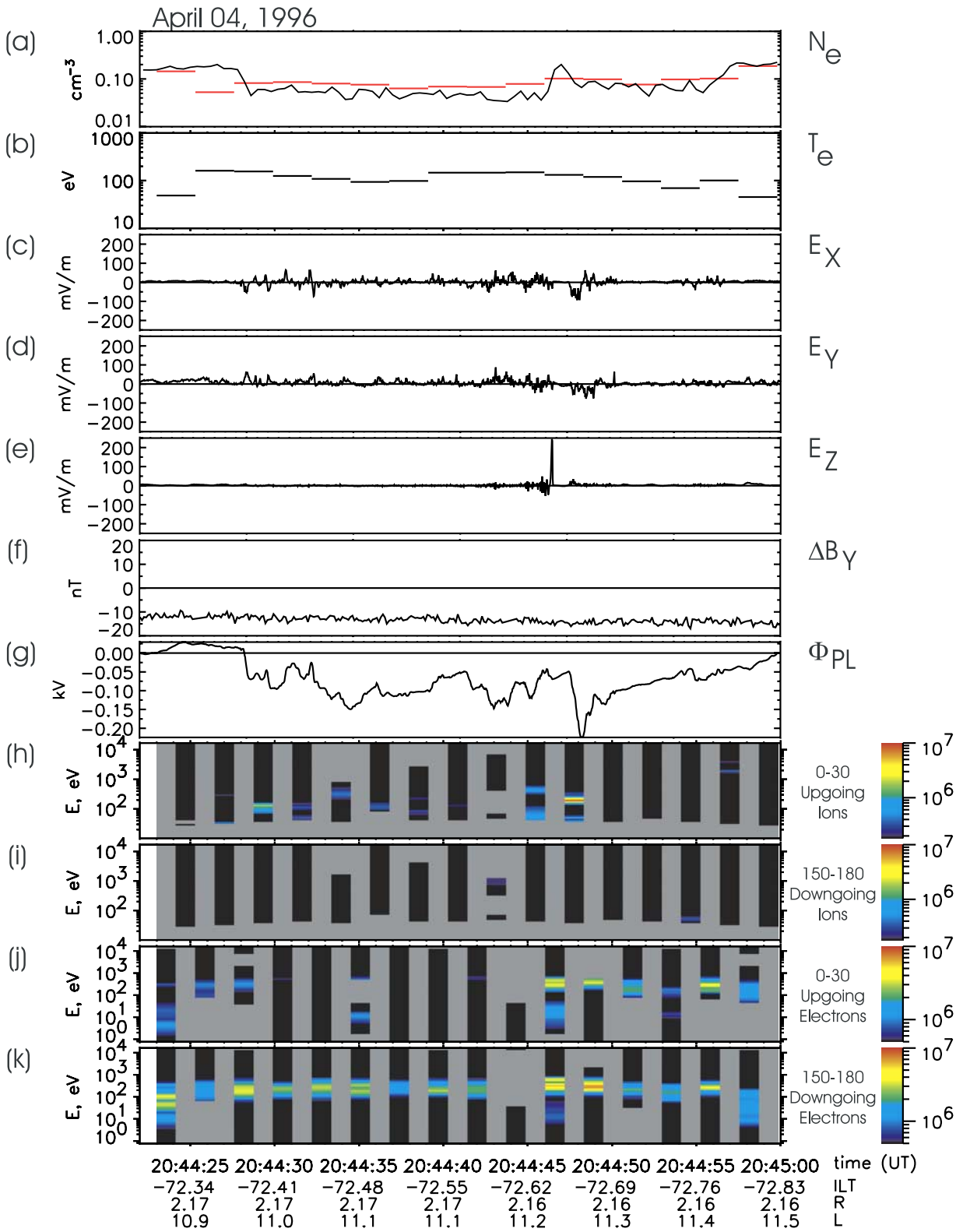

Figure 5. Depicts a southern auroral zone crossing near local midnight on 4 April 1996. Shown are (a) electron density, (b) electron temperature, (c)–(e) the components of the electric field vector in field-aligned coordinates, (f) the east-west perturbation magnetic field, (g) the plasma potential, (h)–(i) spectrograms of field-aligned and field-opposed differential ion energy flux, respectively, and (j)–(k) spectrograms of field-aligned and field-opposed differential electron energy flux.

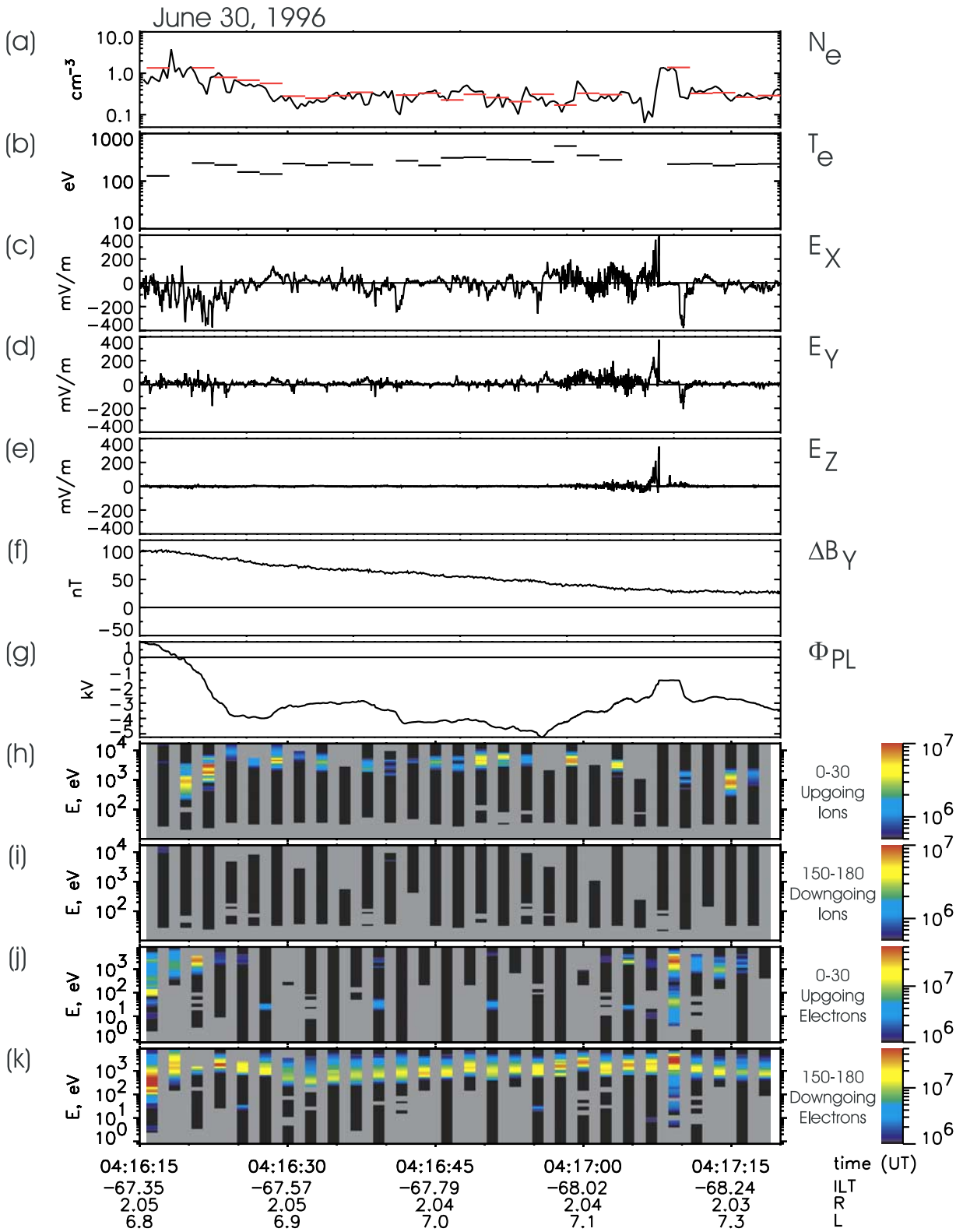

Figure 6. Depicts a southern auroral zone crossing near dusk on 30 June 1996. Shown are (a) electron density, (b) electron temperature, (c)–(e) the components of the electric field vector in field-aligned coordinates, (f) the east-west perturbation magnetic field, (g) the plasma potential, (h)–(i) spectrograms of field-aligned and field-opposed differential ion energy flux, respectively, and (j)–(k) spectrograms of field-aligned and field-opposed differential electron energy flux.

Table 1. Characteristic Parameters

Event/Time	α	dS, km	$dS_{\parallel}$, km	$dS_{\perp}$, km	λ_D, km	c/ω_{pe}, km	r_p, km	$\langle T_e \rangle$, keV	N_{eo}/N_{ei}
04-04-1996/2044:46	11.0°	0.81	0.82	4.4	0.15	16	0.3	0.09	2.9
06-30-1996/0417:07	55.8°	4.6	8.2	5.6	0.2	9	0.5	0.25	8.6
09-25-1996/2347:46	75.4°	5.7	23.0	6.0	0.5	11	0.5	0.85	5.0
12-24-1997/0156:34	77.0°	2.3	10.4	2.4	0.2	6	—	0.5	3.5
05-04-1998/2054:27	76.3°	1.7	7.3	1.8	0.35	17	0.3	0.27	2.0
05-30-1998/0324:33	80.0°	2.0	12.0	2.1	0.2	5	0.3	0.62	3.4[a]
11-03-1998/1805:04	80.0°	6.6	38.2	6.7	0.3	10	0.9	0.85	4.2
11-24-1998/1422:00	76.0°	10.1	41.0	10.5	0.3	7	0.9	1.2	2.5

[a]Estimated from spacecraft potential measurements.

events were sampled at an altitude of $\sim 1R_E$ and most occurred during relatively quiet magnetospheric conditions ($K_p \lesssim 2+$). The characteristics of these eight events are summarized in Table 1. Table 1 gives the dates and times of each event, the angle between the normal and the magnetic field α, the thickness along the normal dS, the corresponding thicknesses parallel and perpendicular to the magnetic field, the Debye length λ_D, the electron inertial length c/ω_{pe}, the gyroradius of an upgoing proton beam r_p, the average electron temperature $\langle T_e \rangle$, and the ratio between the electron density outside the cavity and the electron density within the auroral cavity N_{eo}/N_{ei} in the vicinity of the parallel electric field events. The events are sampled from a variety of field geometries and plasma conditions, with average temperatures ranging from 70 eV to 1.2 keV and density ratios from 2 to 8.6. The thicknesses of the layers containing parallel electric fields range from about 0.8 to 10 km, which suggest the existence of significant parallel potential drops concentrated in regions that are tens of kilometers in extent given the geometries sampled.

[33] The square of the electron thermal Mach numbers given in the second column of Table 2 suggest that electron inertial effects are negligible compared with electron pressure gradient effects. The predicted values for the parallel electric field $\langle E_{\parallel} \rangle^{\text{pred}}$ computed using equation (8) and the observed average values parallel electric field $\langle E_{\parallel} \rangle^{\text{obs}}$ are given in the third and fourth columns of Table 2, respectively. The predicted values for the parallel electric field computed using equation (8) are in good agreement with the values of the parallel electric field averaged over the layer proper. These favorable comparisons provide strong evidence that the large-amplitude parallel electric field structures are supported by sharp gradients in the electron pressure along the magnetic fields, with the dominant contribution to the pressure gradient coming from the gradient in the electron density. Mechanisms, such as electron inertia [e.g., *Rönnmark*, 1999] and the effects of mirroring magnetic fields on differential electron and ion anisotropy [e.g., *Alfvén and Fälthammer*, 1963] to explain small amplitude parallel electric fields, which are believed to be responsible for a significant potential drop distributed over thousands of kilometers, cannot explain these large-amplitude, macroscopic parallel electric fields, which lead to a large potential drop localized in a region that is roughly tens of kilometers in extent along the magnetic field. Although the steady state description of the parallel electric field is analogous to modeling the electrons as a Boltzmann response to the parallel electric field, it is not a priori obvious that this is an appropriate description of the equilibrium fields in a collisionless plasma, where the electron distribution function is nonthermal.

5.1. Relation to Alfvén Waves

[34] Alfvén waves have been suggested as a possible source of the parallel electric fields responsible for accelerating the plasma in the auroral acceleration region [e.g., *Hasegawa*, 1976; *Goertz and Boswell*, 1979; *Lysak and Lotko*, 1996; *Lysak*, 1998; *Stasiewicz et al.*, 2000, and references therein]. Moreover, Alfvén waves can appear to be electrostatic, especially for structures that are sufficiently narrow in the direction transverse to the magnetic field. *Hull et al.* [2003] demonstrated that the Alfvén wave description was not feasible by showing that the predicted ratio $\nu = V_A B_Y / E_X$ obtained from Figure 1 of the paper by *Lysak* [1998] is one to two orders of magnitude larger than actually observed. However, *Hull et al.* [2003] were only able to apply this test to one event. Here we show that the parallel electric fields in the events discussed in this paper are not likely to be due to purely propagating dispersive Alfvén waves.

[35] The parallel electric field events are observed at an altitude of $\sim 1R_E$. At these altitudes, $V_A/V_{the} \gg 1$ and therefore inertial effects predominate over kinetic effects in an Alfvén wave description. Purely propagating Alfvén plane waves in an infinite homogeneous plasma where

Table 2. Summary Test Results

Event/Time	M_{the}^2	$\langle E_{\parallel} \rangle^{\text{pred}}$, mV/m	$\langle E_{\parallel} \rangle^{\text{obs}}$, mV/m	ϵ^{Alf}	ϵ^{Obs}	f^{Alf}, Hz	f^{Obs}, Hz
04-04-1996/2044:46	0.048	117 ± 77	80	5.4	6 ± 4	2×10^4	4.2
06-30-1996/0417:07	0.036	66 ± 40	102	0.68	0.3 ± 0.2	2.5×10^3	1.5
09-25-1996/2347:46	0.040	59 ± 10	50	0.26	0.21 ± 0.13	1.4×10^3	1.0
12-24-1997/0156:34	0.026	60 ± 12	61	0.23	0.25 ± 0.10	1.3×10^3	2.8
05-04-1998/2054:27	0.26	25 ± 15	39	0.25	0.3 ± 0.1	2×10^4	0.4
05-30-1998/0324:33	0.023	64 ± 38	48	0.17	0.22 ± 0.17	1.7×10^3	2.9
11-03-1998/1805:04	0.026	32 ± 13	21	0.18	0.16 ± 0.11	5×10^2	0.5
11-24-1998/1422:00	0.006	27 ± 11	21	0.26	0.22 ± 0.12	5×10^1	0.5

inertial effects are important obey the dispersion relation given by:

$$\omega/k_{\|} = V_A\sqrt{\frac{1}{1+k_{\perp}^2\lambda_e^2}}, \tag{11}$$

where V_A is the Alfvén speed and ω is the wave frequency, $k_{\perp}$ and $k_{\|}$ represent wave numbers perpendicular and parallel to the magnetic field, and λ_e is the electron inertial length. The ratio between the parallel and perpendicular components of the electric field are given by:

$$\epsilon^{\mathrm{Alf}} = \frac{E_{\|}}{E_{\perp}} = \frac{k_{\|}}{k_{\perp}}, \tag{12}$$

in the limit $k_{\perp}^2\lambda_e^2 \gg 1$. As a necessary but not sufficient condition for this simple purely propagating Alfvén wave model to be a valid description of the parallel electric fields in the events considered in this study, both equations (11) and (12) must be satisfied.

[36] Under the approximation that $k_{\|} \approx 2\pi/dS_{\|}$ and $k_{\perp} \approx 2\pi/dS_{\perp}$, we find that equation (12) yields Alfvén wave predicted values of the ratio ϵ^{Alf} that are in reasonable agreement with the observed average values of the ratio ϵ^{Obs}. Values for ϵ^{Alf} and ϵ^{Obs} are summarized in the fifth and sixth columns of Table 2. However, equation (11) predicts wave frequencies that are typically two to four orders of magnitude too large. Under the conditions over which the parallel electric field structures are observed, an Alfvén wave pulse will occur in the frequency range from $f^{\mathrm{Alf}} = 50$ Hz to 2×10^4 Hz, whereas the large-amplitude, macroscopic parallel electric fields are observed to occur in the frequency range from $f^{\mathrm{Obs}} = 0.4$ Hz to 4.2 Hz (see Table 2). Moreover, waves that occur at such high f^{Alf} are outside the scope of purely propagating dispersive Alfvén wave theory (e.g., they are not Alfvén waves). Thus we conclude that a purely propagating Alfvén plane wave cannot explain the parallel electric field signatures.

[37] It is important to note that the effects of Alfvén wave reflection off of sharp gradients in the plasma density along the magnetic field have not been treated in models of the acceleration region. More recent studies have described the properties of Alfvén waves in density gradients that vary smoothly over 1 R_E [e.g., *Streltsov and Lotko*, 1999; *Chaston et al.*, 2002, 2003]. For example, the inertial Alfvén wave field-line resonance model of *Streltsov and Lotko* [1999] does have time scales of seconds, however the potential drop is distributed over thousands of kilometers along the field line. Alfvén waves are expected to steepen along the magnetic field and reflect off of the region containing sharp density gradients. Such a process could potentially lead to significant parallel electric fields characterized by short perpendicular and parallel length scales. A model incorporating the effects of sharp density gradients along the magnetic field-line could possibly explain these observations, however the development of such a model is beyond the scope of this paper and is left for future work.

5.2. A Possible Explanation

[38] A possible explanation of the layers is that they are time stationary, magnetized oblique sheath-like structures or magnetized oblique double layers [*Borovsky*, 1983, 1993; *Ergun et al.*, 2002] that form at the boundary between a high and low density plasma, similar to that encountered in laboratory experimental devices. Such structures have thicknesses that are typically tens of Debye lengths [e.g., *Borovsky*, 1983] irrespective of field geometry. The thicknesses of the observed field structures listed in Table 1 are on the order of $10\lambda_D$, which is consistent with a sheath. Moreover, such structures can give rise to significant electric field strengths and hence potential drops extending over these short scales and can explain much of the electric field and particle properties observed in the auroral acceleration zone [*Borovsky*, 1993; *Ergun et al.*, 2002]. In particular the numerical solution to 1-D Vlasov-Poisson equations [*Ergun et al.*, 2002] constrained by boundary conditions appropriate to the auroral zone resulted in an asymmetric electric field signature in the region marked by a strong gradient in the plasma density, which is consistent with the observations presented in this paper. It is important to note that this asymmetric character is apparent in roughly 66% of the 64 events presented by *Hull et al.* [2003]. The remaining 34% either do not appear to display this asymmetry or have more complicated structure, which is obscuring such behavior, if present. Nevertheless, the ability of the double layer model to recover much of the observed features makes this an attractive description of the events discussed in this paper.

6. Summary and Conclusions

[39] We have investigated the properties of large-amplitude macroscopic parallel electric fields observed in the upward current part of the auroral acceleration region. Thickness estimates suggest that the large-amplitude parallel field structures are highly localized both parallel (e.g., tens of kilometers as opposed to thousands of kilometers) and perpendicular to the magnetic field. We provided evidence that suggests that these localized parallel electric fields are predominantly balanced by electron pressure gradients along the magnetic field line, with electron pressure anisotropy, electron inertia, and resistivity possibly providing higher-order corrections. More accurate estimates of the distribution of the parallel electric field in the layer requires the electron density and temperature and corresponding gradients to be resolved in the layer (e.g., an order of magnitude improvement in Hydra's DDEIS time sampling). These structures do not appear to be due to purely propagating Alfvén waves. A more likely explanation is that the large-amplitude parallel fields are a sheath field that forms at the interface along the magnetic field separating plasmas of different densities and temperatures. These large quasistationary fields provide a significant fraction of the auroral acceleration zone potential drop and therefore are an integral part of the field structure responsible for the acceleration of particles in the auroral acceleration region, as suggested in earlier theoretical and observational studies.

[40] **Acknowledgments.** We thank C. T. Russell for the generous free use of the Polar magnetometer data. The work at UC Berkeley was supported by NASA grants NAG5-3182 and NAG5-12039. Partial support for this work for J.D.S. from NASA grant NAG5-7883 is also acknowledged.

[41] Arthur Richmond thanks Joseph Borovsky and Philip L. Pritchett for their assistance in evaluating this paper.

References

Alfvén, H., and C. G. Fälthammer, *Cosmical Electrodynamics*, 2nd ed., Clarendon, Oxford, UK, 1963.

Borovsky, J. E., The scaling of oblique plasma double layers, *Phys. Fluids*, *26*, 3273–3278, 1983.

Borovsky, J. E., The strong-double-layer model of auroral arcs: An assessment, in *Auroral Plasma Dynamics*, *Geophys. Monogr. Ser.*, vol. 80, edited by R. L. Lysak, pp. 113–120, AGU, Washington, D. C., 1993.

Cattell, C., et al., The association of electrostatic ion cyclotron waves, ion and electron beams and field-aligned currents: FAST observations of an auroral zone crossing near midnight, *Geophys. Res. Lett.*, *25*, 2053–2056, 1998a.

Cattell, C. A., J. R. Wygant, J. Dombeck, F. S. Mozer, M. A. Temerin, and C. T. Russell, Observations of large-amplitude parallel electric field wave packets at the plasma sheet boundary, *Geophys. Res. Lett.*, *25*, 857–860, 1998b.

Chaston, C. C., J. W. Bonnell, C. W. Carlson, M. Berthomier, L. M. Peticolas, I. Roth, J. P. McFadden, R. E. Ergun, and R. J. Strangeway, Electron acceleration in the ionospheric Alfvén resonator, *J. Geophys. Res.*, *107*(A11), 1413, doi:10.1029/2002JA009272, 2002.

Chaston, C. C., J. W. Bonnell, C. W. Carlson, R. J. Strangeway, J. P. McFadden, and R. E. Ergun, Kinetic effects in the acceleration of auroral electrons in small scale Alfvén waves: A FAST case study, *Geophys. Res. Lett.*, *30*(6), 1289, doi:10.1029/2002GL015777, 2003.

Ergun, R. E., et al., FAST satellite observations of electric field structures in the auroral zone, *Geophys. Res. Lett.*, *25*, 2025–2028, 1998.

Ergun, R. E., C. W. Carlson, J. P. McFadden, F. S. Mozer, and R. J. Strangeway, Parallel electric fields in discrete arcs, *Geophys. Res. Lett.*, *27*, 4053–4056, 2000.

Ergun, R. E., Y. J. Su, L. Andersson, C. W. Carlson, J. P. McFadden, F. S. Mozer, D. L. Newman, M. V. Goldman, and R. J. Strangeway, Direct observations of localized parallel electric fields in a space plasma, *Phys. Rev. Lett.*, *87*, 5003, 2001.

Ergun, R. E., L. Andersson, D. Main, Y.-J. Su, D. L. Newmann, M. V. Goldman, C. W. Carlson, J. P. McFadden, and F. S. Mozer, Parallel electric fields in the upward current region of the aurora: Numerical solutions, *Phys. Plasmas*, *9*, 3695–3704, 2002.

Escoubet, C. P., A. Pedersen, R. Schmidt, and P. A. Lindqvist, Density in the magnetosphere inferred from ISEE 1 spacecraft potential, *J. Geophys. Res.*, *102*, 17,595–17,609, 1997.

Goertz, C. K., and R. W. Boswell, Magnetosphere-ionosphere coupling, *J. Geophys. Res.*, *84*, 7239–7246, 1979.

Goodrich, C. C., and J. D. Scudder, The adiabatic energy change of plasma electrons and the frame dependence of the cross-shock potential at collisionless magnetosonic shock waves, *J. Geophys. Res.*, *89*, 6654–6662, 1984.

Harvey, P., et al., The electric field instrument on the Polar satellite, *Space Sci. Rev.*, *71*, 583–596, 1995.

Hasegawa, A., Particle acceleration by mhd surface wave and formation of aurora, *J. Geophys. Res.*, *81*, 5083–5090, 1976.

Hudson, M. K., R. L. Lysak, and F. S. Mozer, Magnetic field-aligned potential drops due to electrostatic ion cyclotron turbulence, *Geophys. Res. Lett.*, *5*, 143–146, 1978.

Hull, A. J., F. S. Mozer, and J. W. Bonnell, Statistical survey of large amplitude parallel electric fields observed in the auroral acceleration region by polar, *Eos Trans. AGU*, *81*(48), Fall Meet. Suppl., F1009, 2000a.

Hull, A. J., J. D. Scudder, R. J. Fitzenreiter, K. W. Ogilvie, J. A. Newbury, and C. T. Russell, Electron temperature and de Hoffmann-Teller potential change across the Earth's bow shock: New results from ISEE 1, *J. Geophys. Res.*, *105*, 20,957–20,971, 2000b.

Hull, A. J., J. W. Bonnell, F. S. Mozer, and J. D. Scudder, A statistical study of large-amplitude parallel electric fields in the upward current region of the auroral acceleration region, *J. Geophys. Res.*, *108*(A1), 1007, doi:10.1029/2001JA007540, 2003.

Kintner, P. M., M. C. Kelley, R. D. Sharp, A. G. Ghielmetti, M. Temerin, C. Cattell, P. F. Mizera, and J. F. Fennell, Simultaneous observations of energetic (keV) upstreaming ions and electrostatic hydrogen cyclotron waves, *J. Geophys. Res.*, *84*, 7201–7212, 1979.

Lysak, R. L., The relationship between electrostatic shocks and kinetic Alfvén waves, *Geophys. Res. Lett.*, *25*, 2089–2092, 1998.

Lysak, R. L., and W. Lotko, On the dispersion relation for shear Alfvén waves, *J. Geophys. Res.*, *101*, 5085–5094, 1996.

Mozer, F. S., On the lowest altitude S3-3 observations of electrostatic shocks and parallel electric fields, *Geophys. Res. Lett.*, *7*, 1097–1098, 1980.

Mozer, F. S., and A. Hull, The origin and geometry of upward parallel electric fields in the auroral acceleration region, *J. Geophys. Res.*, *106*, 5763–5778, 2001.

Mozer, F. S., and C. A. Kletzing, Direct observation of large, quasi-static, parallel electric fields in the auroral acceleration region, *Geophys. Res. Lett.*, *25*, 1629–1632, 1998.

Mozer, F. S., C. W. Carlson, M. K. Hudson, R. B. Torbert, B. Parady, J. Yatteau, and M. C. Kelley, Observations of paired electrostatic shocks in the polar magnetosphere, *Phys. Rev. Lett.*, *38*, 292–295, 1977.

Mozer, F. S., C. A. Cattell, M. K. Hudson, R. L. Lysak, M. Temerin, and R. B. Torbert, Satellite measurments and theories of low altitude auroral particle acceleration, *Space Sci. Rev.*, *27*, 155–213, 1980.

Pannekoek, A., Ionization in stellar atmospheres, *Bull. Astron. Neth.*, *1*, 107–118, 1922.

Rönnmark, K., Electron acceleration in the auroral current circuit, *Geophys. Res. Lett.*, *26*, 983–986, 1999.

Rosseland, S., Electrical state of a star, *Mon. Not. R. Astron. Soc.*, *84*, 720–728, 1924.

Russell, C. T., R. C. Snare, J. D. Means, D. Pierce, D. Dearborn, M. Larson, G. Barr, and G. Le, The GGS/Polar magnetic fields investigation, *Space Sci. Rev.*, *71*, 563–582, 1995.

Scudder, J., et al., Hydra—A three-dimensional electron and ion hot plasma instrument for the Polar spacecraft of the GGS mission, *Space Sci. Rev.*, *71*, 459–495, 1995.

Scudder, J. D., A. Mangeney, C. Lacombe, C. C. Harvey, C. Wu, and R. Anderson, The resolved layer of a collisionless, high β, supercritical, quasi-perpendicular shock wave: 3. Vlasov electrodynamics, *J. Geophys. Res.*, *91*, 11,074–11,097, 1986.

Scudder, J. D., F. S. Mozer, N. C. Maynard, and C. T. Russell, Fingerprints of collisionless reconnection at the separator: 1. Ambipolar-Hall signatures, *J. Geophys. Res.*, *107*(A10), 1294, doi:10.1029/2001JA000126, 2002.

Stasiewicz, K., et al., Small scale Alfvénic structure in the aurora, *Space Sci. Rev.*, *92*, 423–533, 2000.

Streltsov, A. V., and W. Lotko, Small-scale, "electrostatic" auroral structures and Alfvén waves, *J. Geophys. Res.*, *104*, 4411–4426, 1999.

Treumann, R. A., and W. Baumjohann, *Advanced Space Plasma Physics*, Imperial College Press, London, 1997.

J. W. Bonnell, C. C. Chaston, A. J. Hull, and F. S. Mozer, Space Sciences Laboratory, University of California, Berkeley, CA 94720, USA. (jbonnell@ssl.berkeley.edu; ccc@ssl.berkeley.edu; ahull@ssl.berkeley.edu; fmozer@ssl.berkeley.edu)

J. D. Scudder, Department of Physics and Astronomy, University of Iowa, Iowa City, IA 52242, USA. (jds@space-theory.physics.uiowa.edu)